

Article

A New Double-Step Process of Shortening Fibers without Change in Molding Equipment Followed by Electron Beam to Strengthen Short Glass Fiber Reinforced Polyester BMC

Michael C. Faudree ^{1,*}  and Yoshitake Nishi ²¹ Faculty of Liberal Arts and Science, Tokyo City University, Yokohama-shi 224-8551, Japan² Graduate School of Engineering, Tokai University, Hiratsuka-shi 259-1292, Japan; west@tsc.u-tokai.ac.jp

* Correspondence: faudree@tcu.ac.jp

Abstract: It is vital to maximize the safety of outdoor constructions, airplanes, and space vehicles by protecting against the impact of airborne debris from increasing winds due to climate change, or from bird strikes or micrometeoroids. In a widely-used compression-molded short glass fiber polyester bulk-molded compound (SGFRP-BMC) with 55% wt. CaCO₃ filler, the center of the mother panel has lower impact strength than the outer sections with solidification texture angles and short glass fiber (SGF) orientations being random from 0 to 90 degrees. Therefore, a new double-step process of: (1) reducing commercial fiber length without change in molding equipment; followed by a (2) 0.86 MGy dose of homogeneous low-voltage electron beam irradiation (HLEBI) to both sides of the finished samples requiring no chemicals or additives, which is shown to increase the Charpy impact value (a_{uc}) about 50% from 6.26 to 9.59 kJm⁻² at median-accumulative probability of fracture, $P_f = 0.500$. Shortening the SGFs results in higher fiber spacing density, S_f , as the thermal compressive stress site proliferation by action of the CTE difference between the matrix and SGF while the composite cools and shrinks. To boost impact strength further, HLEBI provides additional nano-compressive stresses by generating dangling bonds (DBs) creating repulsive forces while increasing SGF/matrix adhesion. Increased internal cracking apparently occurs, raising the a_{uc} .

Keywords: SGFRP; BMC; impact strength; fiber length; texture; electron beam irradiation

Citation: Faudree, M.C.; Nishi, Y. A New Double-Step Process of Shortening Fibers without Change in Molding Equipment Followed by Electron Beam to Strengthen Short Glass Fiber Reinforced Polyester BMC. *Materials* **2024**, *17*, 2036. <https://doi.org/10.3390/ma17092036>

Academic Editor: Andrea Bernasconi

Received: 23 February 2024

Revised: 19 April 2024

Accepted: 24 April 2024

Published: 26 April 2024



Copyright: © 2024 by the authors. Licensee MDPI, Basel, Switzerland. This article is an open access article distributed under the terms and conditions of the Creative Commons Attribution (CC BY) license (<https://creativecommons.org/licenses/by/4.0/>).

1. Introduction

With the increase in frequency and intensity of disaster events from climate change, it is important to advance materials that can withstand the increasingly harsh environmental conditions that can occur. It is crucial to always strengthen materials for maximum safety, with the utmost concern for the environment. Bulk molded compounds (BMCs) have been widely-used across many industries for light-load bearing articles, such as electrical housing, car headlights, and appliance parts. BMCs have advantages over metals in being corrosion resistant and lightweight when used as non-structural parts for aircraft or other vehicles to lower fuel consumption and reduce CO₂ emissions. Other advantages are their easy formability of complex shaped parts, and their resistance to hot or cold for house appliances and outdoor household articles. BMCs usually have fiber content of ~5 to 30 wt.% [1–12] which includes glass [11,12], carbon [13], as well as jute [14] and kenaf [15]. Short glass fiber reinforced polymer–bulk molded compounds (SGFRP-BMCs) are 3-phase fiber-filler-polymer systems constructed with fiber at ~5 to 30 wt.% [1,3,7] and filler of CaCO₃ at ~35 to 55 wt.% [7,8]. For BMCs in general, fillers of TiO₂, Al₂O₃, SiC, Mg(OH)₂, ZnO [9], fumed silica [10], fly ash [5], or waste thermosetting BMC [2] have been used.

Up to now, the combination of shortening fibers and electron beam treatment to enhance mechanical properties of fiber reinforced polymers (FRPs) has not been found in the literature. However, other strengthening methods have always been advancing for

FRPs [16–25]. For example, for long fiber FRP, pre-stressing fibers before intrusion with the polymer melt has been a useful tool to increase mechanical properties [16–19]. Similar to pre-stressing steel bars in concrete, Pang and Fancey found viscoelastic prestressing of multi-filament nylon 6,6 yarn in a bisphenol-A-based low viscosity epoxy resin increased tensile strength, modulus, and toughness up to 15%, 30%, and 40%, respectively [16]. For a unidirectional glass fiber reinforced polymer (GFRP) epoxy composite, Hadi and Ashton found pre-stressing GFs at 25, 50, 75, 100, and 200 MPa increased tensile strength and elastic modulus [17]. Motahari and Cameron found prestressing fibers increased flexural properties of FRP [18]. Interestingly, Jenkins et al. found by controlling prestressing magnitude and eccentricity, mold-free FRP composites' internal stress conditions can be manipulated to obtain curved part geometry with high precision [19]. Another method commonly used for strengthening FRPs has been enhancing adhesion at the fiber/matrix interface [20–25]. Yuan et al. found that applying good a coupling agent to GFs increased fracture stress, but decreased fracture strain in polyvinyl chloride (PVC) GFRP [20]. Meraghni et al. modelled the effect of interfacial degradation on a short fiber-reinforced polymer containing matrix microcracks [21]. Numerous fiber treatments have been applied to inert CF to increase its weak adhesion to polymer matrix [22–25], including electrochemical modification [22], electro-polymer coating [23], plasma surface modification [24], and Ni sputtering [25].

Past research has shown the mechanical properties of 2-phase fiber/polymer FRP systems that shortening fiber length decreases mechanical properties such as impact strength, tensile stress, and strain [26–34], and that longer fibers are desired [35]. For example, in a polypropylene (PP) GFRP at GF wt.% from 3 to 60%, stiffness was found to be lower at shorter fiber lengths below 0.5 mm, and virtually unchanged above 0.5 mm [26]. Above 40 wt.% GF content, modulus was lowered by fiber packing problems and increased in voids [26]. Another study of PP GFRP showed that impact strength was increased as GF length was raised to 6.4 mm, with a strain energy model predicting optimal length to be 8 mm [28]. In a PP carbon fiber reinforced polymer (CFRP), a sequential reduction in mechanical properties, Izod impact, tensile strength and modulus, bending strength and modulus, and Rockwell hardness were found as CF length was reduced from 10 to 5 to 2 to 1 to 0.5 mm [32]. In a CFRP, tensile strength and stiffness were increased by lengthening CF from 2 to 4 mm, but were decreased as CF length was increased further to 6.4 mm. Optimal fiber length was reported to be 4 mm [33]. Numerical modeling has also been carried out on 2-phase GFRP systems showing that as GFs are lengthened, strength increases rapidly at low fiber lengths, especially near the critical length, l_c of ~ 1.0 mm, and flattens out at about $5l_c$ [29,30]. Fu and Lauke calculated l_c to be 0.56–0.59 mm for nylon FRP, 1.4 mm for polypropylene (PP) FRP, and 0.68 to 0.84 mm for polybutylene terephthalate (PBI) FRP [29]. For 2-phase systems, below l_c , fibers do not impart stress transfer to the matrix, i.e., they are too short to exhibit shear lag with the matrix during tension. Hence, instead of breakage, the dominant fracture mechanism for fibers below l_c is pull-out, weakening the 2-phase fiber/polymer system. However, with the 3-phase fiber-filler-polymer system, CTE difference is the dominant mechanism, where shortening fibers to 0.44 mm strengthens, rather than weakens, the composite [36]. For green composites also (2-phase), a trend was found, being that lowering fiber length decreases mechanical strength, such as those with hemp fiber (HF) [34,37], jute fiber (JF) [38,39], sisal fiber (SF) [40], or agave fiber (AF) [41]. For example, in HF-reinforced thermoplastic polyurethane (HFRP), tensile strength was raised from 16 to peak out at 27 MPa by lengthening HFs from 6 mm to 15 mm [34]. However, above 15 mm to 40 mm, tensile strength remained approximately constant [34]. In injection-molded poly[styrene-*b*-(ethylene-co-butylene)-*b*-styrene] (SEBS)/HFRP composite with 30 wt.% HF, increasing nominal fiber length from 1.10 mm to 4.19 mm (from 0.57 mm to 1.03 mm after injection molding) significantly raised tensile strength from ~ 33 to ~ 39 MPa, and tensile modulus from ~ 2.3 to ~ 2.9 GPa [37]. Sajin et al. found for a compression molded alkali-treated JF-reinforced isophthalic polyester composite (JFRP), 20 mm fiber length gave the highest tensile strength and modulus, flexural strength and modulus, and impact strength. The 20 mm fiber length samples had higher mechanical properties than either the

5, 10, 15, or 25 mm samples [39]. In a compression-molded sisal fiber-reinforced PP (SFRP) composite with 40 wt.% SF, increasing chopped SF length from ~5 mm to ~25 mm (from ~3 mm to ~17 mm after compounding) resulted in increase in tensile strength from ~36 to ~43 MPa, flexural strength from ~41 to ~62 MPa, flexural modulus from 1.4 to ~2.9 GPa, and impact strength from 3.25 to 4.09 kJm⁻² [40]. Moreover, for a biodegradable composite fabricated from agave leaves and epoxy (AFRP), longer AF lengths of 60 mm were found to give better tensile and flexural properties than those that were 10 mm or chopped [41]. Hence, in 2-phase fiber-polymer systems, mechanical properties typically decrease with a decrease in fiber length.

However, counter to the results stated in the literature for numerous 2-phase fiber/polymer composite systems, in the 3-phase SGFRP-BMC, several mechanical properties have been increased by decreasing fiber length below that of commercially used samples [7,8,36]. For a widely-used compression-molded styrene butadiene SGFRP-BMC with 11 wt.% SGF and 55 wt.% CaCO₃ filler, it was found that shortening SGF length from nominal (commercial) 6.4 mm to submillimeter 0.44 mm raised impact strength 25% at the typically weak center of the mother panel [36]. Moreover, for an injection-molded styrene-butadiene SGFRP-BMC with 20 wt.% SGF, and 47.1 wt.% CaCO₃ filler, shortening SGFs from 6.4 mm to 0.44 mm increased tensile modulus 5 to 25% [8]. Ultimate tensile strength (UTS) and its strain were also boosted by ~60 and ~40%, respectively [7]. This was unusual, since there is typically a tradeoff: as UTS is enhanced, its strain is typically decreased [16]. Other mechanical tests, such as flexural and fatigue, would provide a more thorough characterization, but are beyond the scope of this study.

In the above cases, SGFs were shortened by 30 min in an extended mix of the paste in a sigma-blade mixer prior to molding without a change in molding equipment. Enhancements by shortening fibers has been described with a “fiber spacing” model [8] depicted in Figure 1. For the simple case when fibers are separated by spaces in a given length, x , number of fibers, N_f will be equivalent to number of spaces, S_f , as shown in Equation (1):

$$S_f = N_f \quad (1)$$

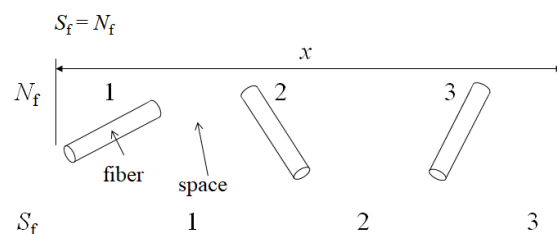


Figure 1. Fiber spacing model adapted from Faudree et al. (2014) [8].

This would be independent of fiber orientation, θ , with respect to x . And apply to the random fiber orientation of the SGFRP-BMC panel center. Moreover, since both N_f and S_f are dimensionless quantities, they can be put into any dimensional coordinate system; hence, S_f is given in three dimensions as “fiber spacing density” (mm⁻³).

Enhancements of mechanical properties were attributed to the increase in S_f as mean fiber length, l_f (mm) is shortened, acting to increase the micro-compressive stress sites of the matrix on the SGFs by a difference in coefficient of thermal expansion (CTE) during cooling down and shrinking [8]. S_f is related to l_f by the following Equation [8]:

$$S_f = \rho_f = V_f / (\pi r^2 l_f) \quad (2)$$

where V_f and r are SGF volume fraction and mean fiber radius (0.007 mm). It follows that the CTE of cured polyester resin matrix is 55 to 100 × 10⁻⁶/K [42], an order of magnitude above E-glass fibers at 5.4 × 10⁻⁶/K [43]. In concert with this, since the SGFRP-BMC is a three-phase fiber-filler-polymer system, the filled matrix behaves as a polymer-filler subsystem in the narrow spacing between fibers that efficiently allows for an increase in

mechanical properties by decreasing the fiber length. During cooling down and shrinking, the polymer compresses onto the hard CaCO_3 filler with a high surface area of the 1 to 7 μm CaCO_3 particles, whose listed CTE is $\sim 4.6 \times 10^{-6}/\text{K}$ [44]. As S_f is increased by reducing SGF length, micro-compressive stress sites are increased, raising the mechanical properties.

Note that in the SGFRP-BMC under study, V_f of hard components of SGFs plus CaCO_3 filler is quite high at 46%, with the polymer mixture at 54%. Small particles that are highly dispersed and in close proximity are excellent for maximizing thermal residual stresses [45] for strengthening the BMC composites. Another point here is in the case of boosting the ultimate tensile stress and strain; the increase in S_f also acts to halt cracks before propagating above the critical length for the SGFRP-BMC to take on more of the load [7]. Therefore, for the 3-phase SGFRP-BMC, shortening the fiber length has been found to increase mechanical properties.

Other studies on shorter fiber lengths increasing mechanical properties are nearly non-existent. However, Senthilrajan et al. found, for a jute reinforced polyester (JFRP), at JF content of 25 wt.%, 5 mm fiber length samples had higher flexural strength and modulus, and a specific strength and modulus than those with longer lengths of 10, 15, 20, or 25 mm [38]. Their scanning electron microscope (SEM) analysis attributed the strengthening to stronger JF/Matrix bonding [38].

As mentioned previously, the CaCO_3 filler particles of the SGFRP-BMC appear to act to raise tensile strength and its strain, along with tensile modulus, and impact strength when SGF length is reduced [7,8]. Metal matrix composites (MMC) and cemented carbide composites, as well as ceramics, are reported to exhibit this strengthening mechanism, in that reduced particle size increases mechanical properties [46–48]. Improvements were attributed to increased residual compressive stress sites by the CTE mismatch between the particles and the matrix. In the SGFRP-BMC, CaCO_3 filler particles were measured using SEM to be in about the same size range, <1 to 7 μm [8], as that for ceramics at <1 μm to several microns [46–48].

Concerning the influence of filler on BMCs, little research has been performed in the literature. An important study for sustainability for hard-to-recycle BMCs was conducted by Matykiewicz et al., who crushed waste thermosetting BMC, using it as reinforcement in an epoxy composite [2]. Lautenschlägera et al. investigated the effects of filler for 25 vol.% jute chopped fiber-reinforced BMCs and needle-punched non-woven SMCs [14]. They showed that CaCO_3 filler was found to produce higher tensile strength and Young's modulus than that of paltry kaolin. In contrast, they found flexural strength had high scatter for either filler, due to inhomogeneous fiber distribution of fiber-rich and -sparse volumes [14]. Investigations on the effect of percent filler is beyond the scope of this study.

In injection-molded SGFRP-BMC, the mean SGF length of 30 min extended mix samples was measured using SEM to be sub-millimeter at 0.44 mm (std. dev. = ± 0.203 mm) [1,7]. Thus, it is assumed, for the compression molded samples, that the 30 min mixing reduces SGF length to about 0.44 mm. With standard deviation of ± 0.203 mm, SGF length difference between the 30 min extended mix compression-molded samples and commercial 6.4 mm samples is considered enough to obtain reliable results [7,8]. Notably, the sub-millimeter length is below that of the estimated l_c of ~ 1.0 mm reported for 2-phase FRPs [29,30], and l_c would depend on adhesion strength at the fiber/matrix interface. The extended mixing of 30 min is reported to have insignificant effect on the CaCO_3 filler particles (<1 to ~ 7 μm) [2].

To boost impact strength further, homogeneous low-voltage electron beam (HLEBI) treatment to finished specimens with the shortened 0.44 mm SGFs will be employed. This is because, previously, 0.86 MGy HLEBI treatment to commercial 6.4 mm samples was found to increase impact values from 5 to 25% [49]. SEM showed that 0.86 MGy HLEBI resulted in much more polymer/ CaCO_3 matrix adhering to the SGFs than that of untreated, which were left virtually bare. An electron spin resonance (ESR) analysis of the samples showed HLEBI generated a strong peak (inflection point at 323.0 mT) signifying the presence of dangling bonds (DBs). The DBs are lone pair electrons in the outer orbital shells that exhibit repulsive forces acting to increase internal micro-compressive stress

sites, and strengthen the SGF/Matrix interface [49]. This allows for energy dispersion in the form of higher numbers of cracks generated in the SGFRP-BMC samples to take on higher energy impacts [49]. An examination of tested samples showed that the fracture mechanism transitioned at a_{uc} of 5.4 to 6.7 kJm^{-2} from clean to smaller secondary micro-crack proliferation, sometimes including bends near the main crack. Fracture surface area was observed to increase with increasing impact strength. The conversion was independent of HLEBI-treated or untreated conditions [49].

HLEBI has a positive track record of enhancing GFRPs with long fibers, GFs themselves, silica glass, and several types of polymers [49,50]. HLEBI is also reported to strengthen the fiber/matrix interface with electronic charge generation and the formation of DBs [49].

HLEBI typically severs bonds with the lowest BDE (Figure 2a,b) for polymeric components in the SGFRP-BMC. DBs are formed at the terminated atoms with low BDE [49] in methylene groups ($\text{CH}_2\text{-CH}_2$: 369 kJmol^{-1}), hydroxyl groups ($\text{CH}_3\text{-OH}$: 377 kJmol^{-1}), and phenyl groups ($\text{C}_6\text{H}_5\text{-R}$: <377~389 kJmol^{-1} where R- is $\text{CH}_3\text{-}$ or $\text{C}_2\text{H}_5\text{-}$). Free-radical hydrogens have higher BDE (H-CH : 427 kJmol^{-1} , $\text{H-OC}_2\text{H}_5$: 435 kJmol^{-1} , and H-OOCCH_3 : 469 kJmol^{-1}). Alkene groups $\text{H}_2\text{C=CH}_2$ have the highest BDE at 720 kJmol^{-1} [51,52].

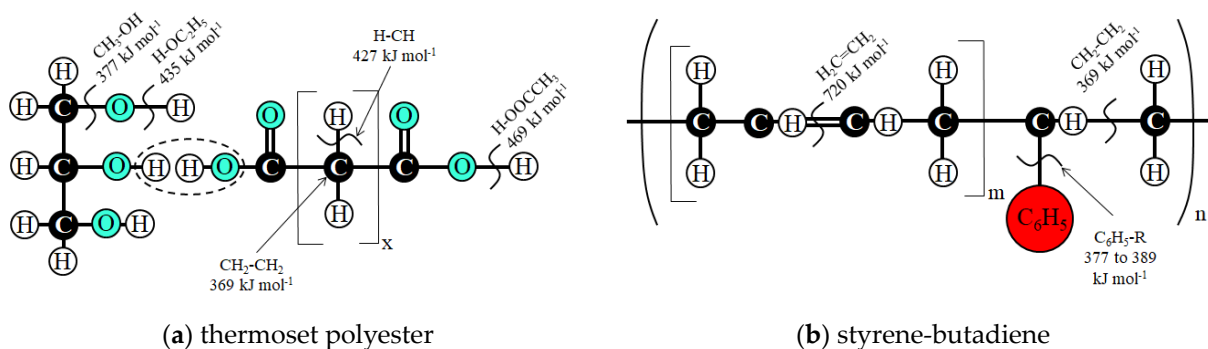


Figure 2. Depiction of HLEBI-activated: (a) thermoset polyester, and (b) styrene-butadiene copolymer, respectively, adapted from Faudree et al. (2012) [49], indicating approximate bond dissociation energies (BDE) [51,52] and DBs.

The action of HLEBI results in atoms being spaced further apart by DB generation, creating compressive stress sites by repulsion of the generated lone-pair electrons. For silica glass, for instance, in the radial distribution function (RDF), the normalized coordination number (N_D/N_O) is reduced, while the normalized mean atomic distance, (r_D/r_O) is increased [49]. This results in nano-scale volume expansion that can act to increase mechanical properties.

As mentioned earlier, we strengthen the weak center of the SGFRP-BMC panel by shortening SGFs followed by HLEBI. This is because separate studies of shortening SGFs from commercial 6.4 mm to 0.44 mm [36]; and applying 0.86 MGy HLEBI to finished 6.4 mm samples [49] were found to successfully raise impact energy of the weak center of the SGFRP-BMC mother panel, 25%, and 5 to 25%, respectively. Hence, it seems possible that the combination can additively boost impact strength by 50%. Therefore, we chose the independent parameters of (1) 6.4 mm SGFs, (2) 0.44 mm, and (3) 0.44 mm + 0.86 HLEBI to illustrate the enhancements. The 6.4 mm is chosen since it is widely used commercially, while the 0.44 mm was found to yield significant increase in mechanical properties [7,36]. In addition, the 0.86 MGy HLEBI dose was chosen since preliminary testing showed that it produced the highest impact values out of a wide range of dose levels [49]. Therefore, the goal of this study is to apply a double-step process of (1) shortening the nominal 6.4 mm fiber length formulation to 0.44 mm by 30 min extended mixing without change in molding equipment, followed by (2) applying a 0.86 MGy dose of HLEBI to both sides of the SFGRP-BMC finished samples with no chemicals or additives to boost impact values at the weak center of the mother panel.

2. Materials and Methods

2.1. Preparation of SGFRP-BMC Samples

Compression-molded SGFRP-BMC panels were provided by Premix, Inc., (now Citadel Plastics) North Kingsville, OH, USA, with components listed in Table 1. A strong coupling agent was used on the SGFs, but its components are proprietary. Processing parameters, panel geometry, and volume fractions are listed in Table 2. A schematic of the compression molding process is illustrated in Figure 3, where SGFs are mixed into a paste prior to injection molding. The test matrix is composed of three data sets listed in Table 3 designated as “6.4 mm”, “0.44 mm”, and “0.44 mm + HLEBI” samples. The “6.4 mm” data set is the commercial formulation SGFRP-BMC with nominal 6.4 mm SGFs which underwent 20 min mixing of the paste with a double-arm sigma blade Banbury mixer before injection molding. The “0.44 mm” are those with an extended mix of 30 min, equaling 50 min mixing total. Mean SGF length was found to be 0.44 mm [36]. The 6.4 mm and 0.44 mm samples were not treated with HLEBI. A third data set, the “0.44 mm + HLEBI”, was treated with 0.86 MGy HLEBI on both sides of the finished samples.

Table 1. Weight percents of SGFRP-BMC components.

COMPONENT	Wt. %
Propylene glycol maleate polyester	13.75
Styrene butadiene copolymer	12.75
Commercial E-glass fibers	11
CaCO ₃ filler	55
Aluminum silicate filler	3
Magnesium hydroxide	0.5
Proprietary initiators and inhibitors	4

Table 2. Processing parameters.

PARAMETER	Condition
Mold pressure	5.5 to 6.9 MPa (800 to 1000 psi)
Temperature	422 K (149 °C)
Cure time	2 min
Mold type	Matched metal die compression mold
Panel size	304.8 × 304.8 mm (12 × 12 in)
Panel thickness	2 mm
V_f (SGF)	0.080
V_f (CaCO ₃)	0.377
V_f (remaining polymer mixture)	0.543

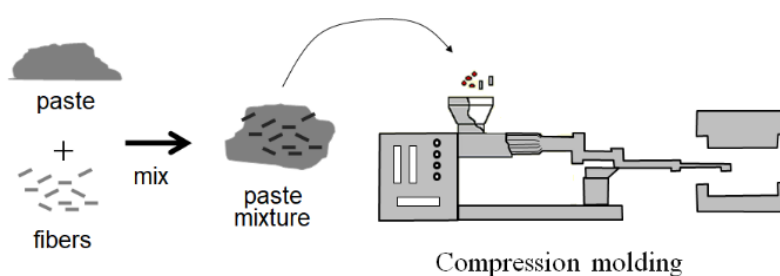


Figure 3. Schematic of compression molding process.

Table 3. Data sets of the SGFRP-BMC.

Experimental Condition	6.4 mm Untreated	0.44 mm Untreated	0.44 mm + HLEBI
Number of Specimens	14	14	14

Figure 4 shows the fabrication steps for the three data sets, (a) 6.4 mm, (b) 0.44 mm, and (c) 0.44 mm + HLEBI. The commercial 6.4 mm and 0.44 mm samples were fabricated in three and four steps, respectively [36]. Figure 4 shows that the 0.44 mm + HLEBI samples were fabricated in five steps. Step 1 is mixing the paste for 20 min. Step 2 is 30 min of extended mixing. Step 3 is compression molding the paste into panels. Step 4 is cutting the samples. Finally, Step 5 is applying 0.86 MGy HLEBI to both sides of the samples (see the HLEBI Section).

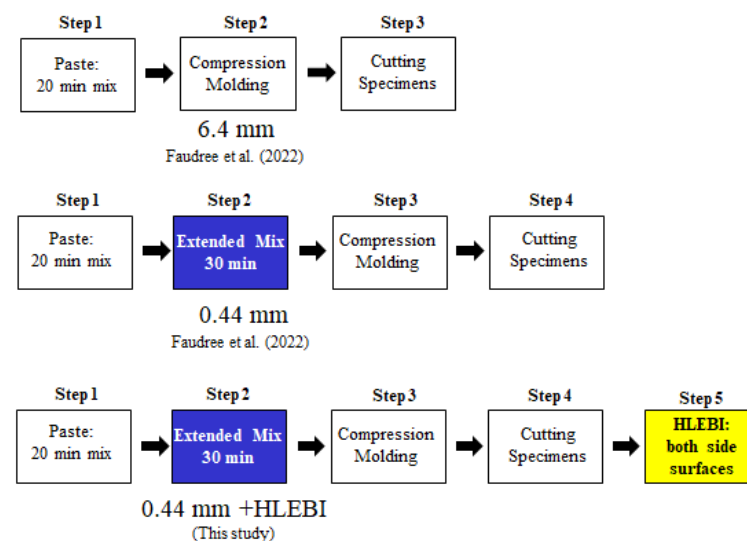


Figure 4. Steps of SGFRP-BMC fabrication for 6.4 mm; 0.44 mm (Faudree et al. (2022)) [36]; and 0.44 mm + HLEBI samples, respectively.

Figure 5 is an illustration of the SGFRP-BMC panels, showing specimens taken from the weak center section. During compression molding of the paste charge, the direction of flow is outward, but more random just below the plunger in the center. After molding, specimens ($80 \times 10 \times 2$ mm) were cut according to ASTM D 6110-02 (2002) [53] for anisotropic panels [53]. Since this study focusses on improving impact strength at the weak panel center, samples cut from outer 3 sub-quadrants of each quadrant are not shown. Only the 4 sub-quadrants at center are shown, and are assumed to have identical flow patterns since they exhibited statistically lower impact strength than the outer sections [1,36,49]. Locations of samples cut from the panel center are indicated in Figure 5. For consistency, specimens in each sub-quadrant are numbered from 1 to 7 outward from the center. The 14-sample data sets were taken from two sub-quadrants, two each from sample numbers 1 to 7.

2.2. Homogeneous Low-Voltage Electron Beam Irradiation

After molding and cutting, samples were treated with a HLEBI processor (Table 4) (Type LB250/15/180L, Energy Science, Inc., Woburn, MA, USA, Iwasaki Electric Group, Ltd., Tokyo, Japan), as shown in Figure 6a,b [49]. Faudree et al. (2022) gives a detailed explanation [36]. To estimate how far into sample thickness HLEBI activates, penetration

depth, D_{th} (μm) is calculated. When ρ is sample density (g cm^{-3}) and V is acceleration voltage at sample surface (kV), the D_{th} can be obtained [54]:

$$D_{th} = 66.7V^{5/3}/\rho \tag{3}$$

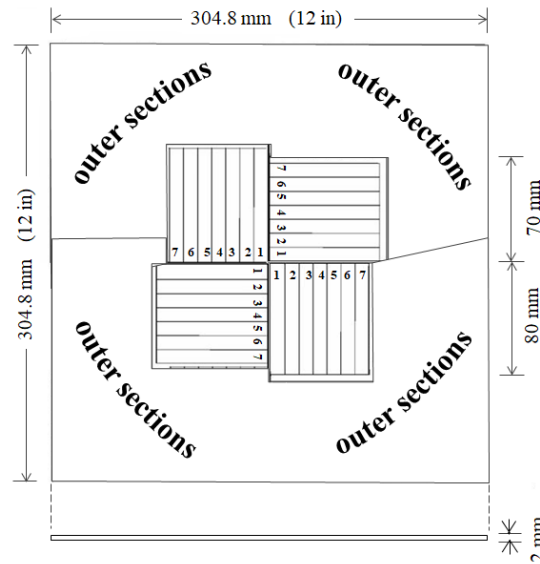


Figure 5. Schematic of Charpy impact sample cutting from the weak center section of a SGFRP-BMC panel. Specimen numbers indicated. (outer section specimens not shown).

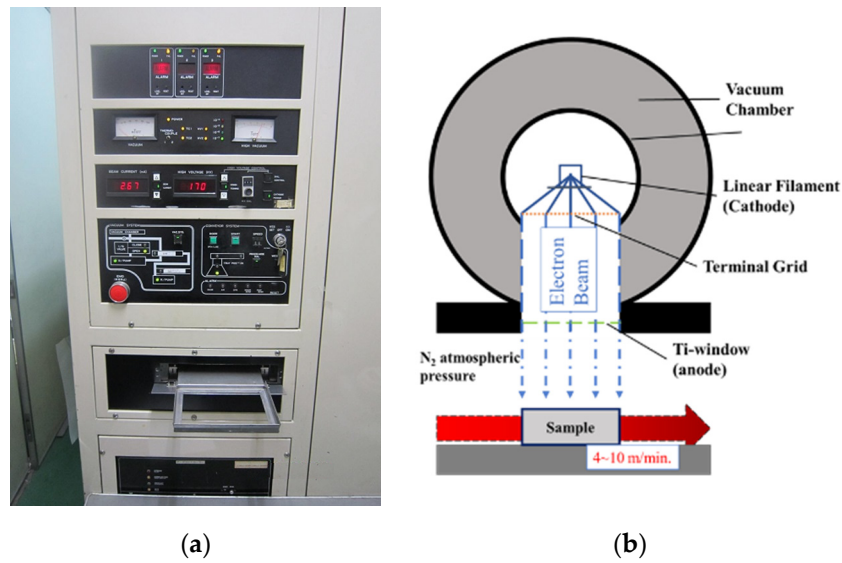


Figure 6. Electron-curtain processor (Iwasaki): (a) photo, and (b) schematic.

Table 4. HLEBI parameters.

Acceleration voltage	170 kV
Irradiating current	2.68 mA
Irradiation environment	N2 gas atmosphere
Residual O ₂ conc.	<300 ppm
Conveyor speed	10 m min ⁻¹
EB dose/sweep	0.0432 MGy
Sweep time (one way)	0.20 s

Table 4. *Cont.*

Gap interval bet. sweeps	20 s
EB yield calc.	FWT Nylon dosimeter

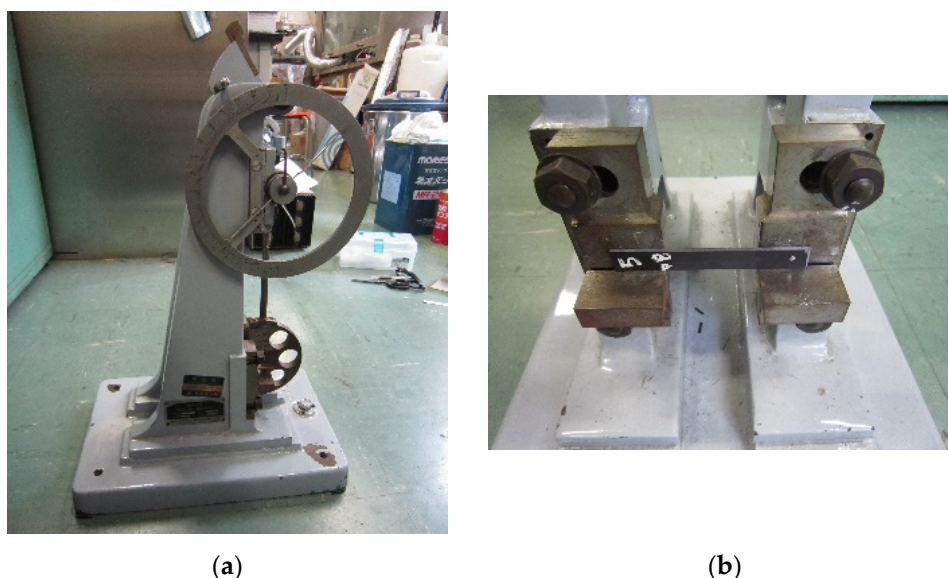
Individual D_{th} are listed in Table 5. D_{th} for the SGFRP-BMC is 116 μm , or about 5.8% into the thickness. Since both specimen sides are HLEBI-activated, there is a skin/core/skin sandwich structure of 0.116/1.87/0.116 mm. Impact tests were carried out 30 ± 0.5 h after HLEBI irradiations.

Table 5. Densities and the calculated D_{th} for the SGFRP-BMC (bold type) and its individual components [54].

Component	Density, ρ (g cm^{-3})	D_{th} (μm)
Polymer Mixture	1.200	185
Matrix Compos.	1.847	120
SGFRP-BMC	1.917	116
SGF	2.620	84.5
CaCO ₃ Filler	2.800	79.1

2.3. Charpy Impact Tests

Charpy impact strength was measured using a drop-weight pendulum apparatus (Shimadzu Corp. No. 51735, Tokyo, Japan) [55,56] according to the JIS K 7077-1991 testing standard [55]. Figure 7a,b shows the impact tester and specimen mount. Specimen dimensions were $80 \times 10 \times 2$ mm. Testing parameters and details can be found in Faudree et al. (2022) [36].

**Figure 7.** Photos of: (a) Charpy impact tester, and (b) mount with SGFRP-BMC specimen.

3. Results

Effect of Shortening SGFs and HLEBI on Impact Values

Experimental results are shown in Figure 8a,b for the 6.4 mm (black dots), 0.44 mm (blue triangles) [36], and 0.44 mm + HLEBI (yellow squares) samples, respectively. Figure 8a shows accumulative probabilities (P_f) vs. Charpy impact value (a_{uc}) according to a general form of the median rank method [57] described in detail in Faudree et al. (2022) [36]. Figure 8a shows, for the 0.44 + HLEBI data set, our double-step process of (1) shortening

fibers to 0.44 mm with 30 min extended mixing, followed by (2) HLEBI of 0.86 MGy, boosted a_{uc} at all P_f over that of the 6.4 mm. The 0.44 mm data set (without HLEBI, blue triangles) is from a previous study reported by Faudree et al. (2022) [36], and is shown here to illustrate that the 0.44 mm + HLEBI data set yields higher a_{uc} than the 0.44 mm at all P_f . Although at low- P_f of 0.049, a_{uc} of the 0.44 mm data set was reduced (4.06 kJm⁻²) from that of the 6.4 mm (4.92 kJm⁻²) [36], the 0.44 mm + HLEBI process showed a significant improvement to 7.06 kJm⁻². As stated in [36], the a_{uc} are calculated from ($a_{uc} = E/(bt)$) with impact energy, and E is obtained with ($E = WR[(\cos\beta - \cos\alpha) - (\cos\alpha' - \cos\alpha)(\alpha + \beta)/(\alpha - \alpha')]$). The P_f are calculated from ($P_f = (I - 0.3)/(N_s + 0.4)$).

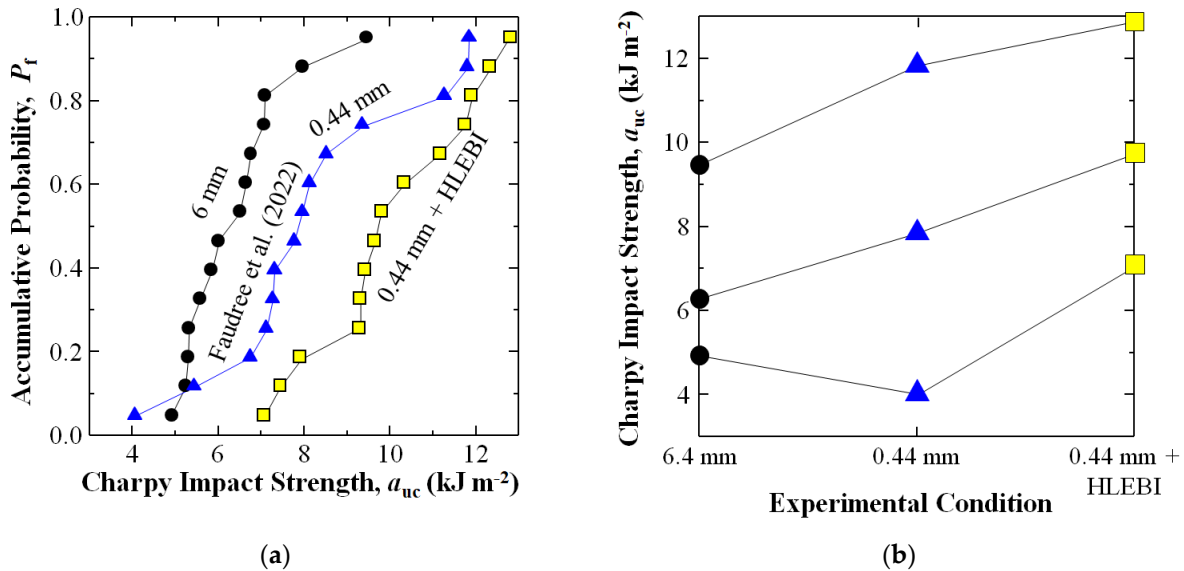


Figure 8. Experimental results showing: (a) changes in Charpy impact values a_{uc} (kJm⁻²) for SGFRP-BMC samples of untreated 6 mm and 0.44 mm, along with 0.44mm + HLEBI (0.86 MGy), with (b) the a_{uc} from (a) a_{uc} at low-, median-, and high- P_f of 0.049, 0.500, and 0.951, respectively. The 0.44 mm data are from Faudree et al. (2022) [36].

Figure 8b shows a_{uc} at low-, median-, and high- P_f of 0.049, 0.500, and 0.951, respectively. Namely, the 0.44 mm + HLEBI data set shows significant increase in a_{uc} over that of 6.4 mm. At P_f of 0.049, 0.500, and 0.951, a_{uc} was increased 43%, 55%, and 35%, respectively, from 4.92 to 7.06 kJm⁻², 6.26 to 9.72 kJm⁻², and 9.45 to 12.80 kJm⁻². For the 0.44 mm data set, Figure 8b shows the increases in a_{uc} at median- and high- P_f , but a decrease at low- P_f of 0.049 compared with those of 6.4 mm [36]. However, the 0.44 mm + HLEBI process significantly raises the a_{uc} over those of the 6.4 mm samples at low- P_f of 0.049, along with those at median-, and high P_f .

Table 6 provides individual a_{uc} for each sample of the data sets in Figure 8.

Table 6. Charpy impact values, a_{uc} (kJm⁻²), of individual specimens along with their accumulative probabilities, P_f .

P_f	6.4 mm Untreated	0.44 mm Untreated	0.44 mm+ HLEBI
0.049	4.92	4.06	7.06
0.118	5.24	5.44	7.45
0.188	5.29	6.74	7.91
0.257	5.32	7.12	9.28
0.326	5.57	7.26	9.30
0.396	5.84	7.31	9.41

Table 6. Cont.

P_f	6.4 mm Untreated	0.44 mm Untreated	0.44 mm+ HLEBI
0.465	6.01	7.76	9.64
0.535	6.51	7.96	9.80
0.604	6.64	8.12	10.33
0.674	6.76	8.51	11.16
0.743	7.06	9.35	11.75
0.813	7.09	11.26	11.89
0.882	7.97	11.79	12.33
0.951	9.45	11.84	12.80

4. Discussion

4.1. Average Impact Strength

Since average values are commonly employed in strength evaluations, Figure 9 is included here showing the average a_{uc} ($a_{uc,avg}$) with standard deviation bars. Figure 9 shows the double-step process of 0.44 mm + HLEBI significantly increased $a_{uc,avg}$ 56% over that of 6.4 mm from 6.41 to 10.00 kJm^{-2} . Although standard deviations were quite high at 1.24 and 1.81 kJm^{-2} for the 6.4 and 0.44 + HLEBI data sets, respectively, the lower limit of the 0.44 mm + HLEBI (8.19 kJm^{-2}) was higher than the upper limit of the 6.4 mm (7.65 kJm^{-2}). This provides further support that our double-step process can apparently increase the a_{uc} of weak center sections of the SGFRP-BMC panels.

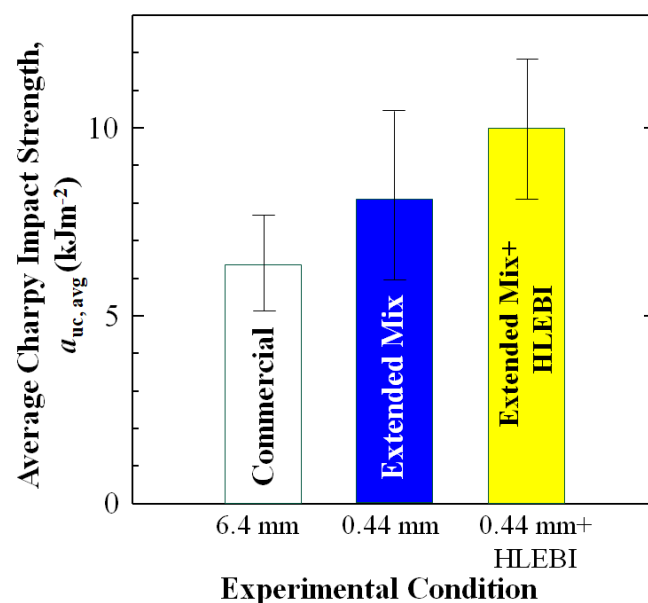


Figure 9. Average impact strength, $a_{uc,avg}$ (kJm^{-2}) with standard deviations (bars) for the three data sets: 6.4 mm, 0.44 mm, and 0.44 mm + HLEBI, respectively.

4.2. Micro-Strengthening Mechanism Using Extended Mix

Figure 10a–c illustrates the micro-strengthening mechanism by an extended mix of the SGFRP-BMC for the 6.4 mm, 0.44 mm, and 0.4 mm + HLEBI specimens. The SGFs are depicted as having a random orientation as in the panel center. Impact strength enhancements are attributed to increase in S_f and N_f , as l_f is shortened, acting to increase micro-compressive stress sites of the matrix on the SGFs by a difference in CTE during cooling down and shrinking [8,36]. The composite is hardened, increasing impact resistance.

Figure 11b shows an order of magnitude increase in S_f and N_f over that of 6.4 mm (a) that is exceptionally more dispersed. Here, N_f is made to approximate the actual situation where a total length of 58 of 0.44 mm SGFs equals 4 of 6.4 mm SGFs. To discuss enhancement during impact, Figure 10 is made to depict tensile side of specimen with impact area across specimen width (dotted lines). Shortening SGFs to 0.44 mm allows for a higher proportion of SGFs to cross the line, along with increased compressive stress sites (arrows), to counter tensile deformation from impact for higher a_{uc} . On the other hand, in Figure 10a, the less dispersed 6.4 mm samples have gaps in the form of areas lacking SGFs with less residual stresses resulting in easier crack initiation and propagation in the matrix at the tensile side when impacted.

Micro-strengthening by extended mix, with overall nano-strengthening by HLEBI

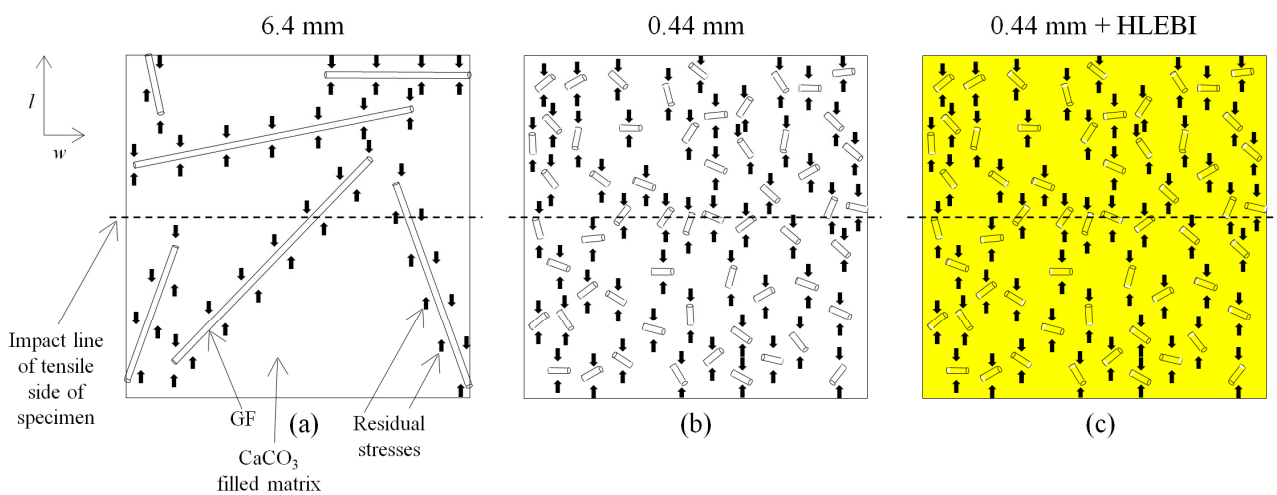


Figure 10. Schematic of micro-scale strengthening mechanism showing (a) 6.4 mm; (b) 0.44 mm; and (c) 0.44 mm + HLEBI samples, respectively. In (c), yellow indicates HLEBI activation. Specimen tensile sides are depicted with line of impact. Specimen length and width directions are indicated.

Nano-strengthening SGF/Matrix interface by HLEBI

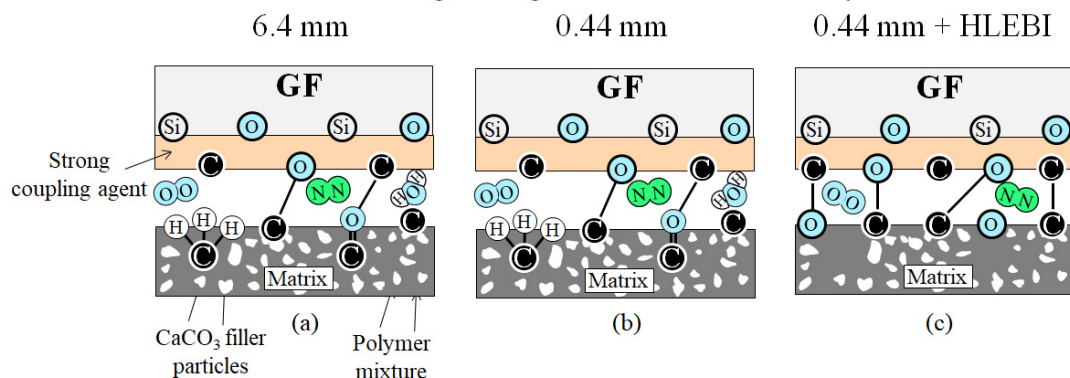


Figure 11. Schematic of the nano-scale SGF/Matrix interface-strengthening mechanism by HLEBI depicting an increase in strong bonds for: (a) 6.4 mm; (b) 0.44 mm; and (c) 0.44 mm + HLEBI samples, respectively.

As mentioned earlier, the filled matrix behaves as a polymer-filler subsystem in the spacing between fibers allowing for an increase, but not a decrease, in mechanical properties with decreasing fiber length. To increase a_{uc} further, Figure 10c depicts the nano-scale strengthening of the 0.44 mm composite with HLEBI represented in yellow.

4.3. Nano-Strengthening Mechanism Using HLEBI

To illustrate the nano-strengthening mechanism, action of HLEBI occurs at: (1) the SGF/Matrix interface; (2) within the SGFs; and (3) within the polymer matrix. These are explained in Figures 11 and 12, and previously in Figure 2a,b. HLEBI works by severing bonds, creating DBs in the form of lone pair electrons that enhance interfacial adhesion and strengthen bulk materials. When 0.86 MGy HLEBI dose is applied to both surfaces of finished SGFRP-BMC samples at the weak panel center, a_{uc} can be raised. Figure 11a,b shows, for untreated 6.4 mm and 0.44 mm, that the SGF/Matrix interface has typical strong chemical bonds between the SGFs and the matrix from the coupling agent. They are apparently accompanied by weak Van der Waals forces with trace atmospheric gasses, O₂, N₂, and H₂O existing at the interface. However, Figure 11c depicts that when HLEBI is applied in the 0.44 mm + HLEBI samples, additional strong bonds of C-C and C-O are apparently formed by lone electron pairs generated, i.e., DBs, raising the a_{uc} . As mentioned earlier, DBs have been detected in 0.86 MGy HLEBI-treated 6.4 mm fiber length SGFRP-BMC as peak generation using ESR analysis in a previous study [49]. Moreover, SEM revealed the HLEBI increased matrix adhering to SGFs, with increased impact values ~5 to 25% [49].

Nano-strengthening within SGFs by HLEBI

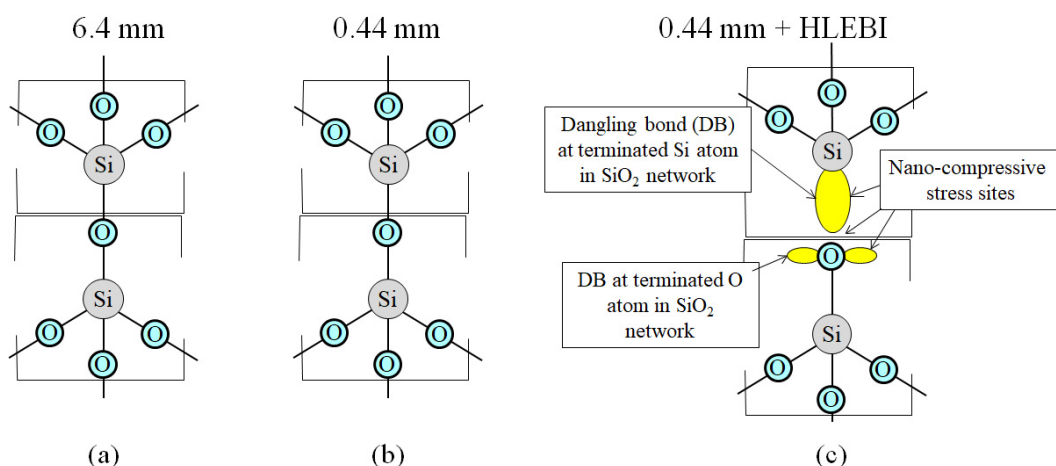


Figure 12. Schematic of the nano-scale strengthening mechanism within SGFs by HLEBI for: (a) 6.4 mm; (b) 0.44 mm; and (c) 0.44 mm + HLEBI samples, respectively.

Figure 12a–c illustrates the strengthening within SGFs by HLEBI. HLEBI has been reported to strengthen silica glass [49]. Figure 12a,b shows the unactivated bonds in the SGFs of 6.4 mm and 0.44 mm samples. However, Figure 12c shows HLEBI activation creates DBs in the outer shell electrons at terminated O atoms in the SiO₂ network in the 0.44 mm + HLEBI samples. The repulsion between lone pairs creates nano-compressive stresses that strengthen SGFs themselves to assist in raising the a_{uc} of the SGFRP-BMC system.

To summarize, the new double-step process of shortening SGFs using a 30 min extended mix, followed by 0.86 MGy HLEBI to finished samples, was found to increase the a_{uc} at the weak center of the SGFRP-BMC compression molded mother panel. This is caused by micro-strengthening by shortening fibers, as well as nano-strengthening by HLEBI.

However, for maximum safety, carefulness is highly recommended, since this study only applies to the panel center. HLEBI to the outer sections may weaken the composite. Also, it is always imperative to test for optimum dose of HLEBI for each situation. Nevertheless, the double-step process was found to increase impact values significantly, over 50%, at the weak center of the SGFRP-BMC mother panel.

4.4. Environmental Sustainability and Long-Term Durability Aspects

With the sharp increase in catastrophic events and heavy degradation to Earth's environment, environmental sustainability must be top priority in manufacture of any product. Therefore, we employ the double-step process to increase the impact strength of the SGFRP-BMC of the 30 min extended mix without a change in molding equipment, followed by HLEBI treatment without the use of any chemicals. However, for a full evaluation of the ecological footprint, life cycle assessment (LCA) is typically carried out. Energy consumption analysis of the double-step process would have to be taken into account. For the LCA to compare that with and without the double-step process would be needed. The LCA is evaluating the continuous cycle of raw materials, manufacturing, transportation, usage and selling, waste disposal, and recycling. The SGFRP-BMC is difficult to recycle, since the polymeric matrix is a thermoset that cannot be melted, for example, to separate it with filler and SGFs. Dumping SGFRP-BMC parts in a landfill is extremely hazardous for the environment and should be strictly prohibited. A highly employed remedy is to ground the waste GFRP-BMC and used as a filler [2]. Use of the filler recycle for thermoplastic FRP would be recommended, since thermoplastics can be repeatedly melted and solidified for recyclability. As for long-term durability assessment, aging studies to check for mechanical strength reduction with time in treated SGFRP-BMC would be needed. LCA and aging studies are beyond the scope of this study, but should be considered for future research.

4.5. Economic Analysis, Scale-Up, and Feasibility Studies

Economic analysis, scale-up, and feasibility information are proprietary and beyond the scope of this study.

5. Conclusions

In order to maximize the safety of outdoor articles, airplanes, and space vehicles by protecting against the impact of airborne debris from increasing winds due to climate change, or from bird strikes or micrometeoroids, it is imperative for composite materials to have high impact resistance. In a 3-phase compression-molded short glass fiber polyester bulk-molded compound (SGFRP-BMC) with 55% wt. CaCO_3 filler and 11% wt. SGF, the center of the mother panel has lower impact strength than the outer sections, with solidification texture angles and SGF orientations being random from 0 to 90 degrees.

1. Therefore, a new double-step process of: (1) shortening the nominal 6.4 mm fiber length formulation to submillimeter 0.44 mm by 30 min extended mixing without change in molding equipment, followed by (2) applying 0.86 MGy dose of homogeneous low-voltage electron beam irradiation (HLEBI) to both sides of the finished samples, requiring no chemicals or additives, which is shown to increase Charpy impact value (a_{uc}) over 50% from 6.26 to 9.59 kJm^{-2} at a median-accumulative probability of fracture, $P_f = 0.500$.
2. Shortening the SGFs by the extended mix method to submillimeter creates a higher number of thermal micro-compressive stress sites between SGF and the matrix to increase impact strength. This is performed by a mismatch of the coefficient of thermal expansion (CTE) between the matrix and fibers acting in the increased fiber spacing density while the composite is undergoing cool-down and shrinkage. In concert with this, since the SGFRP-BMC is a 3-phase fiber-filler-polymer system, the filled matrix behaves as a polymer-filler subsystem in the narrow spacing between fibers that efficiently allows for the increase in mechanical properties by decreasing the fiber length.
3. To boost impact strength further, HLEBI additionally provides nano-compressive stresses in the matrix by generating a dangling bond, which acts as repulsive force site between the outer-shell lone-pair electrons. This, along with increasing SGF/matrix adhesion, occurs with the optimum dose of HLEBI. During impact, a higher degree of internal cracking apparently occurs, raising the impact strength of SFGFRP-BMC samples.

Author Contributions: Conceptualization, M.C.F.; methodology, M.C.F. and Y.N.; software, M.C.F.; validation, M.C.F. and Y.N.; formal analysis, M.C.F.; investigation, M.C.F.; resources, M.C.F. and Y.N.; data curation, M.C.F.; writing—original draft preparation, M.C.F.; writing—review and editing, M.C.F. and Y.N.; visualization, M.C.F.; supervision, Y.N.; project administration, Y.N.; funding acquisition, Y.N. All authors have read and agreed to the published version of the manuscript.

Funding: This research received no external funding.

Institutional Review Board Statement: Not applicable.

Informed Consent Statement: Not applicable.

Data Availability Statement: Experimental data for this manuscript can be obtained upon request by contacting M.C. Faudree of Tokyo City University (faudree@tcu.ac.jp) or Yoshitake Nishi of Tokai University (west@tsc.u-tokai.ac.jp).

Acknowledgments: Shota Iizuka M.S., of Tokai University is acknowledged for his excellent assistance with HLEBI equipment. Sincere appreciation goes to Naoya Tsuchikura, Keisuke Iwata and Masae Kanda for their valuable input. Sincere gratitude goes to Citadel Plastics.

Conflicts of Interest: The authors declare no conflicts of interest.

Abbreviations

The following abbreviations are used in this manuscript.

SGFRP-BMC	short glass fiber reinforced polymer bulk molding compound
SGF	short glass fiber
CTE	coefficient of thermal expansion
HLEBI	homogeneous low-voltage electron beam irradiation
DB	dangling bond
FRP	fiber-reinforced polymer

Symbols

a_{uc}	Charpy impact strength (kJm^{-2})
S_f	fiber spacing density (mm^{-3})
N_f	fiber number density (mm^{-3})
V_f	volume fraction
r	fiber radius (mm)
l_f	fiber length (mm)
BDE	bond dissociation energy (kJ mol^{-1})
D	HLEBI irradiation dose (MGy)
I	HLEBI irradiation current (mA)
S	HLEBI conveyor speed (mmin^{-1})
N	HLEBI number of irradiations
D_{th}	HLEBI penetration depth (μm)
V	HLEBI acceleration voltage (V)
ρ	sample density (g mm^{-3})
E	impact fracture energy (kJ)
W	impact hammer mass (kg)
R	length of hammer weight point from pivot center (m)
β	maximum angle after impact (Rad)
α	start angle before impact (Rad)
α'	maximum angle of a blank test (Rad)
b	specimen width (mm)
t	specimen thickness (mm)
P_f	accumulative probability
I_R	ascending strength rank
N_s	total number of samples in a data set

References

1. Faudree, M.; Nishi, Y.; Gruskiewicz, M.; Salvia, M. A new glass fibered reinforced composite with improved Charpy impact properties at low and high temperatures beyond the extremes of aircraft flight. *Mater. Trans.* **2018**, *59*, 1280–1287. [[CrossRef](#)]
2. Matykiewicz, D.; Barczewski, M.; Sterzyński, T. Morphology and thermomechanical properties of epoxy composites highly filled with waste bulk molding compounds (BMC). *J. Polym. Eng.* **2015**, *35*, 805–811. [[CrossRef](#)]
3. DeRosa, R.; Telfeyan, E.; Gaustad, G.; Mayes, S. Strength and microscopic investigation of unsaturated polyester BMC reinforced with SMC-Recyclate. *J. Thermoplast. Compos. Mater.* **2005**, *18*, 333–349. [[CrossRef](#)]
4. Rajae, P.; Ghasemi, F.A.; Fasihi, M.; Saberian, M. Experimental Analysis and Optimization of Mechanical and Physical Properties of Light-Weight Bulk Molding Compound by Design of Experiment. *J. Macromol. Sci. Part B* **2021**, *60*, 237–256. [[CrossRef](#)]
5. Lee, T.; Jeong, K.; Kim, D. Development of a lightweight BMC material using fly ash. *Adv. Compos. Mater.* **2017**, *26*, 55–64. [[CrossRef](#)]
6. Faudree, M.; Nishi, Y.; Gruskiewicz, M. Characterization of velocity profile of highly-filled GFRP-BMC through rectangular-duct shaped specimen during injection molding from SEM fiber orientation mapping. *Mater. Trans.* **2013**, *54*, 1877–1883. [[CrossRef](#)]
7. Faudree, M.C.; Nishi, Y. Tensile Strength Enhancement by Shortening Glass Fibers with Sub-Millimeter Length in Bulk Molding Polymer Compound. *Mater. Trans.* **2010**, *51*, 2304–2310. [[CrossRef](#)]
8. Faudree, M.C.; Nishi, Y.; Gruskiewicz, M. A Novel ‘Fiber Spacing’ Model of Tensile Modulus Enhancement by Shortening Fibers to Sub-Millimeter in an Injection-Molded Glass Fiber Reinforced Polymer Bulk Molding Compound (GFRP-BMC). *Mater. Trans.* **2014**, *55*, 1292–1298. [[CrossRef](#)]
9. Singh, H.; Singh, T. Effect of fillers of various sizes on mechanical characterization of natural fiber polymer hybrid composites: A review. *Mater. Today Proc.* **2019**, *18*, 5345–5350. [[CrossRef](#)]
10. Rajae, P.; Ghasemi, F.A.; Fasihi, M.; Saberian, M. Effect of styrene-butadiene rubber and fumed silica nano-filler on the microstructure and mechanical properties of glass fiber reinforced unsaturated polyester resin. *Compos. Part B Eng.* **2019**, *173*, 106803. [[CrossRef](#)]
11. Faudree, M.; Baer, E.; Hiltner, A.; Collister, J. Characterization of Damage and Fracture Processes in Short Fiber BMC Composites by Acoustic Emission. *J. Compos. Mater.* **1988**, *22*, 1170–1195. [[CrossRef](#)]
12. Tadlaoui, S.; Granger, R.; Vergnaud, J.M. Correlation Between Dynamic Mechanical Properties and State of Cure for Bulk Moulding Compounds. *Polym. Test.* **1994**, *13*, 271–284. [[CrossRef](#)]
13. Saburov, O.; Huether, J.; Maertens, R.; Trauth, A.; Kechaou, Y.; Henning, F.; Weidenmann, K.A. Adirect process to reuse dry fiber production waste for recycled carbon fiber bulk molding compounds. *Procedia CIRP* **2017**, *66*, 265–270. [[CrossRef](#)]
14. Lautenschläger, M.I.; Mayer, L.; Gebauer, J.; Weidenmanna, K.A.; Henning, F.; Elsner, P. Comparison of filler-dependent mechanical properties of jute fiber reinforced sheet and bulk molding compound. *Compos. Struct.* **2018**, *203*, 960–967. [[CrossRef](#)]
15. Sreenivasan, S.; Sulaiman, S.; Ariffin, M.K.A.M.; Baharudin, B.T.H.T.; Abdan, K. Physical Properties of Novel Kenaf Short Fiber Reinforced Bulk Molding Compounds (BMC) For Compression Moulding. *Mater. Today Proc.* **2018**, *5*, 1226–1232. [[CrossRef](#)]
16. Pang, J.W.C.; Fancey, K.S. Analysis of the tensile behaviour of viscoelastically prestressed polymeric matrix composites. *Compos. Sci. Technol.* **2008**, *68*, 1903–1910. [[CrossRef](#)]
17. Hadi, A.S.; Ashton, J.N. On the influence of pre-stress on the mechanical properties of a unidirectional GRE composite. *Compos. Struct.* **1997**, *40*, 305–311. [[CrossRef](#)]
18. Motahari, S.; Cameron, J. Fibre prestressed composites: Improvement of flexural properties through fibre prestressing. *J. Reinf. Plast. Compos.* **1999**, *18*, 279–288. [[CrossRef](#)]
19. Jenkins, C.; Donough, M.J.; Prusty, B.G. Mould free laminated composites using eccentric fibre prestressing. *Compos. Struct.* **2024**, *331*, 117867. [[CrossRef](#)]
20. Yuan, J.; Hiltner, A.; Baer, E.; Rahrig, R. The mechanical behaviour of PVC short-fibre composites. *J. Mater. Sci.* **1985**, *20*, 4377–4386. [[CrossRef](#)]
21. Meraghni, F.; Blakeman, C.J.; Benzeggagh, M.L. Effect of Interfacial Decohesion on Stiffness Reduction in a Random Discontinuous-Fibre Composite Containing Matrix Microcracks. *Compos. Sci. Technol.* **1996**, *56*, 541–555. [[CrossRef](#)]
22. Pittman, C.U.; Jiang, W.; Yue, Z.R.; Gardner, S.; Wang, L.; Toghiani, H.; Lyon y Leon, C.A. Surface properties of electrochemically oxidized carbon fibers. *Carbon* **1999**, *37*, 1797–1807. [[CrossRef](#)]
23. Hung, K.B.; Li, J.; Fan, Q.; Chen, Z.H. The enhancement of carbon fiber modified with electropolymer coating to the mechanical properties of epoxy resin composites. *Compos. Part A Appl. Sci. Manuf.* **2008**, *39*, 1133–1140. [[CrossRef](#)]
24. Tiwari, S.; Sharma, M.; Panier, S.; Mutel, B.; Mitschang, P.; Bijwe, J. Influence of cold remote nitrogen oxygen plasma treatment on carbon fabric and its composites with specialty polymers. *J. Mater. Sci.* **2011**, *46*, 964–974. [[CrossRef](#)]
25. Faudree, M.C.; Uchida, H.T.; Kimura, H.; Kaneko, S.; Salvia, M.; Nishi, Y. Advances in Titanium/Polymer Hybrid Joints by Carbon Fiber Plug Insert: Current Status and Review. *Materials* **2022**, *15*, 3220. [[CrossRef](#)] [[PubMed](#)]
26. Thomason, J.L.; Vlug, M.A. Influence on fibre length and concentration on the properties of glass fibre reinforced polypropylene: Tensile and flexural modulus. *Compos. Part A Appl. Sci. Manuf.* **1996**, *27*, 477–484. [[CrossRef](#)]
27. Thomason, J. The influence of fibre length, diameter and concentration on the modulus of glass fibre reinforced polyamide 6,6. *Compos. Part A Appl. Sci. Manuf.* **2008**, *39*, 1732–1738. [[CrossRef](#)]
28. Thomason, J.L.; Vlug, M.A. Influence on fibre length and concentration on the properties of glass-fibre-reinforced polypropylene: Impact properties. *J. Compos. Part A* **1997**, *28*, 277–278. [[CrossRef](#)]

29. Fu, S.-Y.; Lauke, B. Effects of fiber length and fiber orientation distributions on the tensile strength of short fiber reinforced polymers. *Compos. Sci. Technol.* **1996**, *56*, 1179–1190. [[CrossRef](#)]
30. Huang, H.; Talreja, R. Numerical simulation of matrix micro-cracking in short fiber reinforced polymer composites: Initiation and propagation. *Compos. Sci. Technol.* **2006**, *66*, 2743–2757. [[CrossRef](#)]
31. Thomason, J.L. The influence of fibre properties of the performance of glass fiber reinforced polyamide 6,6. *Compos. Sci. Technol.* **1999**, *59*, 2315–2328. [[CrossRef](#)]
32. Rezaei, F.; Yunus, R.; Ibrahim, N.A.; Mahdi, E.S. Effect of fiber loading and fiber length on mechanical and thermal properties of short carbon fiber reinforced polypropylene composite. *Malays. J. Anal. Sci.* **2007**, *11*, 181–188.
33. Capela, C.; Oliveira, S.; Pestana, J.; Ferreira, J. Effect of fiber length on the mechanical properties of high dosage carbon reinforced. *Procedia Struct. Integr.* **2017**, *5*, 539–546. [[CrossRef](#)]
34. Haghghatnia, T.; Abbasian, A.; Morshedjani, J. Hemp fiber reinforced thermoplastic polyurethane composite: An investigation in mechanical properties. *Ind. Crops Prod.* **2017**, *108*, 853–863. [[CrossRef](#)]
35. Maertens, R.; Hees, A.; Schöttl, L.; Liebig, W.; Elsner, P.; Weidenmann, K.A. Fiber shortening during injection molding of glass fiber-reinforced phenolic molding compounds: Fiber length measurement method development and validation. *Polym. Technol. Mater.* **2021**, *60*, 872–885. [[CrossRef](#)]
36. Faudree, M.C.; Nishi, Y.; Salvia, M. Increasing Impact Strength of a Short Glass Fiber Compression Molded BMC by Shortening Fibers without Change in Equipment. *Materials* **2022**, *15*, 1145. [[CrossRef](#)] [[PubMed](#)]
37. Panaitescu, D.M.; Fierascu, R.C.; Gabor, A.R.; Nicolae, C.A. Effect of hemp fiber length the mechanical and thermal properties of polypropylene/SEBS/hemp fiber composites. *J. Mater. Res. Technol.* **2020**, *9*, 10768–10781. [[CrossRef](#)]
38. Senthilrajan, S.; Venkateshwaran, N.; Naresh, K.; Velmurugan, R.; Gupta, N.K. Effects of jute fiber length and weight percentage on quasi-static flexural and dynamic mechanical properties of jute/polyester composites for thin-walled structure applications. *Thin-Walled Struct.* **2022**, *179*, 109719.
39. Sajin, J.B.; Christu Paul, R.; Binoj, J.S.; Brailson Mansingh, B.; Gerald Arul Selvan, M.; Goh, K.L.; Rimal Isaac, R.S.; Senthil Saravanan, M.S. Impact of fiber length on mechanical, morphological and thermal analysis of chemical treated jute fiber polymer composites for sustainable applications. *Curr. Res. Green Sustain. Chem.* **2022**, *5*, 10024. [[CrossRef](#)]
40. Bhagat, A.B.; Ghosh, A.K. Estimation of rheological percolation threshold and influence of fibre length on properties of polypropylene/sisal fibre composites having near critical fibre length. *Polymer* **2022**, *258*, 125304. [[CrossRef](#)]
41. Aravinth, K.; Sathish, R.; Ramakrishnan, T.; Balu Mahandiran, S.; Shiyam Sundhar, S. Mechanical investigation of agave fiber reinforced composites based on fiber orientation, fiber length, and fiber volume fraction. *Mater. Today Proc.* **2024**, *in press*. [[CrossRef](#)]
42. Starink, M.; Syngellakis, S. Shear lag models for discontinuous composites: Fibre end stresses and weak interface layers. *Mater. Sci. Eng. A* **1999**, *270*, 270–277. [[CrossRef](#)]
43. Baucio, M.L. (Ed.) *ASM Engineered Materials Reference Book*, 2nd ed.; ASM International: Novelt, OH, USA, 1994.
44. Calcium Carbonate, Calcite (CaCO₃). Available online: https://www.matweb.com/search/datasheet_print.aspx?matguid=bea4bfa9c8bd462093d50da5eebe78ac (accessed on 23 February 2024).
45. Dragoi, D.; Üstündag, E.; Clausen, B.; Bourke, M.A. Investigation of thermal residual stresses in tungsten-fiber/bulk metallic glass matrix composites. *Scr. Mater.* **2001**, *45*, 245–252. [[CrossRef](#)]
46. Seol, K.; Krawitz, A.; Richardson, J.; Weisbrook, C. Effects of WC size and amount on the thermal residual stress in WC–Ni composites. *Mater. Sci. Eng. A* **2005**, *398*, 15–21. [[CrossRef](#)]
47. Niihara, K. Overcoming the fragility of ceramics (Challenge to strengthen ceramics). *Ceram. Kyoujinka Fract. Toughness Ceram.* **1986**, *21*, 581–589. (In Japanese)
48. Wu, C.; Shen, S.; Li, Y.; Luo, G.; Shen, Q.; Gan, Z.; Liu, J. Influence of coarse grain particles on mechanical properties and fracture behavior in multi-modal Al-based metal matrix composites. *Powder Technol.* **2021**, *394*, 901–908. [[CrossRef](#)]
49. Faudree, M.; Nishi, Y.; Gruskiewicz, M. Effects of electron beam irradiation on Charpy impact value of short glass fiber (GFRP) samples with random distribution of solidification texture angles from zero to 90 degrees. *Mater. Trans.* **2012**, *53*, 1412–1419. [[CrossRef](#)]
50. Nishi, Y.; Kobayashi, H.; Salvia, M. Effects of Electron Beam Irradiation on Charpy Impact Value of GFRP. *Mater. Trans.* **2007**, *48*, 1924–1927. [[CrossRef](#)]
51. James, A.; Lord, M. *Macmillan's Chemical and Physical Data, London and Basingstoke*; The Macmillan Press, Ltd.: London and Basingstoke, UK, 1992; pp. 484–485.
52. Gordon, A.; Ford, R. *The Chemists Companion—A handbook of Practical Data, Techniques, and References*; A Wiley Interscience Publication: New York, NY, USA, 1972; pp. 112–113.
53. *ASTM D 6110-02*; Standard Test Methods for Determining the Charpy Impact Resistance of Notched Specimens of Plastics. American Society for Testing and Materials: West Conshohocken, PA, USA, 2002.
54. Christenhusz, R.; Reimer, L. Schichtdickenabhängigkeit der warmerzeugung durch elektronenbestrahlung im energiebereich zwischen 9 und 100 keV (Layer thickness dependency of heat generation by electron irradiation in the energy range between 9 and 100 keV). *Z. Angew. Phys.* **1967**, *23*, 396–404.
55. *JIS K 7077*; Testing Method for Charpy Impact Strength of Carbon Fiber Reinforced Plastics. Japanese Industrial Standards Committee: Tokyo, Japan, 1991. (In Japanese)

56. Splett, J.; Iyer, H.; Wang, C.; McCowan, C. *National Institute of Standards and Technology (NIST) Recommended Practice Guide, Computing Uncertainty for Charpy Impact Test Machine Test Results*; Special publication 960-18; US Department of Commerce: Boulder, Colorado, 2008; pp. 27–29.
57. Nishida, T.; Yasuda, E. *Evaluation of Dynamic Properties of Ceramics (in Japanese, Ceramics no rikigaku tokusei hyouka)*; Nikkan Kogaku Shimbun Sha: Tokyo, Japan, 1986; pp. 50–51.

Disclaimer/Publisher's Note: The statements, opinions and data contained in all publications are solely those of the individual author(s) and contributor(s) and not of MDPI and/or the editor(s). MDPI and/or the editor(s) disclaim responsibility for any injury to people or property resulting from any ideas, methods, instructions or products referred to in the content.